

Three-dimensional theory of the free-electron laser in the collective regime

H. P. Freund* and A. K. Ganguly

Naval Research Laboratory, Washington, D.C. 20375

(Received 23 May 1983)

A fully self-consistent theory of the free-electron laser is derived in the collective regime which includes all transverse variations in the wiggler field as well as the effects of a finite waveguide geometry. A general orbit theory is derived by perturbation about the steady-state trajectories in a configuration which consists of an axial guide field in addition to the helical wiggler field, and used to obtain the source current and charge density for the Maxwell-Poisson equations. By this means, a set of coupled differential equations is found which describes an arbitrary radial beam profile. A dispersion equation is obtained under the assumption of a thin monoenergetic beam, and solved numerically for the growth rates of the TE_{11} and TM_{11} modes in a cylindrical waveguide. A selection rule is found by which the TE_{lm} or TM_{lm} modes are resonant at the l th free-electron-laser Doppler upshift.

I. INTRODUCTION

Interest in the free-electron laser (FEL) as a source of coherent radiation with wavelengths in the millimeter range and below has been maintained by both experimental¹⁻⁸ and theoretical⁹⁻²⁴ studies. Experiments designed to operate in the infrared have, of late, concentrated on the use of a linearly polarized wiggler field composed of permanent magnets.^{5,6} In contrast, experiments at longer wavelengths ($\sim 1-5$ mm) generally make use of helical wiggler fields in concert with an axial guide field. The inclusion of an axial guide field is necessitated by the high currents (~ 1 kA) employed, and such experiments can be made to operate in the collective regime.^{7,8} Theoretical analyses of the helical wiggler FEL experiments have, hitherto, been able to treat the collective regime only in the limit of an idealized one-dimensional wiggler field which is valid only as long as the electron-beam radius is much shorter than the wiggler period.^{9,12-14,17-21,23} A fully self-consistent, three-dimensional theory which includes all transverse variations of the wiggler field as well as the effects of a finite waveguide geometry has recently appeared²⁴; however, it is restricted to the low-gain, single-particle regime. It is our purpose in this work to extend the three-dimensional theory to the collective regime. In contrast, a nonlinear theory has been developed by Colson and Richardson²⁵ for a helical wiggler/pulsed electron-beam configuration. The radiation mode structure is assumed to be that of an optical resonator and is described in a three-dimensional manner; however, the wiggler field and single-particle orbits are described in the idealized limit in which transverse gradients are ignored. In addition, no axial guide field is included in the treatment.

To this end, we first derive the single-particle trajectories of electrons in the self-consistent static magnetic fields by perturbation about the steady-state, helical orbits.^{24,26-28} These orbits are then used to obtain expressions for the source current and charge density which

drive the FEL interaction by solution of the Vlasov equation. The source current and charge density are then used to obtain Maxwell's equations subject to boundary conditions suitable to describe a loss-free cylindrical waveguide. In this manner, a set of differential equations result which model the presence of an arbitrary radial beam profile of electrons which to lowest order execute the steady-state trajectories. In order to obtain analytic solutions to these differential equations, the approximation of a thin beam (i.e., small radial profile) is imposed which is consistent with the assumption of a nearly monoenergetic beam.

The organization of the paper is as follows. The orbit theory is presented in Sec. II, and applied to obtain the source current and charge density in Sec. III. The coupled field equations are derived in Sec. IV for an arbitrary radial profile. The assumption of a thin, monoenergetic beam is imposed in Sec. V and used to obtain and solve the dispersion equation. A summary and discussion is presented in Sec. VI.

II. SINGLE-PARTICLE ORBITS

The physical configuration we employ is that of a relativistic electron beam propagating through an ambient magnetic field composed of a periodic helical wiggler field and a uniform guide field

$$\vec{B}(\vec{x}) = B_0 \hat{e}_z + \vec{B}_w(\vec{x}), \quad (1)$$

where B_0 denotes the magnitude of the guide field, and the wiggler field is taken to be that generated by a bifilar helix²⁷:

$$\vec{B}_w(\vec{x}) = 2B_w [I_1'(\lambda) \cos\chi \hat{e}_r - \lambda^{-1} I_1(\lambda) \sin\chi \hat{e}_\theta + I_1(\lambda) \sin\chi \hat{e}_z]. \quad (2)$$

In Eq. (2), B_w is the amplitude of the wiggler field, $\lambda \equiv k_w r$, $\chi \equiv \theta - k_w z$, $k_w \equiv 2\pi/\lambda_w$ (where λ_w defines the wiggler period), and I_n and I_n' are the modified Bessel

function of the first kind of order n and its derivative, respectively.

The basic equations governing the single-particle orbits in the static magnetic field are

$$\begin{aligned}\gamma\dot{v}_1 &= -[\Omega_0 - \gamma k_w v_3 + 2\Omega_w I_1(\lambda) \sin\chi]v_2 \\ &\quad + \Omega_w v_3 I_2(\lambda) \sin 2\chi, \\ \gamma\dot{v}_2 &= [\Omega_0 - \gamma k_w v_3 + 2\Omega_w I_1(\lambda) \sin\chi]v_1 \\ &\quad - \Omega_w v_3 [I_0(\lambda) + I_2(\lambda) \cos 2\chi], \\ \gamma\dot{v}_3 &= \Omega_w v_2 [I_0(\lambda) + I_2(\lambda) \cos 2\chi] - \Omega_w v_1 I_2(\lambda) \sin 2\chi, \quad (3) \\ \dot{\lambda} &= k_w (v_1 \cos\chi + v_2 \sin\chi), \\ \dot{\chi} &= k_w \lambda^{-1} (-v_1 \sin\chi + v_2 \cos\chi - \lambda v_3),\end{aligned}$$

where $\Omega_{0,w} \equiv |eB_{0,w}/mc|$, $\gamma \equiv (1 - v^2/c^2)^{-1/2}$, and (v_1, v_2, v_3) denote the components of the velocity in a frame rotating with the wiggler and specified by the basis vectors $\hat{e}_1 = \hat{e}_r \cos\chi - \hat{e}_\theta \sin\chi$, $\hat{e}_2 = \hat{e}_r \sin\chi + \hat{e}_\theta \cos\chi$, and $\hat{e}_3 = \hat{e}_z$. It is clear that γ (i.e., the total energy) is a constant of the motion. The class of helical orbits is found by requiring steady-state solutions in which v_1 , v_2 , v_3 , λ , and χ are constants.^{24,27} In this work, the orbits we employ are obtained by expansion about the steady-state trajectories, and a review of the properties of the helical orbits is useful.

The steady-state requirement in (3) results in trajectories in which $v_1 = v_w$, $v_2 = 0$, $v_3 = v_{||}$, $\chi = \pm\pi/2$, and $\lambda = \mp v_w/v_{||}$, where $v_{||} (> 0)$ is a constant and

$$v_w = \frac{2\Omega_w v_{||} I_1(\lambda)/\lambda}{\Omega_0 - \gamma k_w v_{||} \pm 2\Omega_w I_1(\lambda)}. \quad (4)$$

Observe that (4) reduces to the result for an ideal wiggler^{25,27} in the limit as $\lambda \rightarrow 0$. Final determination of the orbit requires knowledge of either v_w , $v_{||}$, or λ (specification of any one of these is sufficient to determine the other two) which, in turn, requires an additional equation relating these quantities:

$$\lambda^2 [(1 - \gamma^{-2})(1 + \lambda^2)^{-1}]^{1/2} = \beta_0 \lambda^2 \pm 2\beta_w (1 + \lambda^2) I_1(\lambda), \quad (5)$$

where $\beta_{0,w} \equiv \Omega_{0,w}/\gamma k_w c$. Solution of these equations produces two distinct classes of trajectory as shown in Fig. 1 in which we plot $v_{||}/c$ vs β_0 (for $\beta_w = 0.05$ and $\gamma = 3.5$). Also shown in the figure are the corresponding solutions in the limit of an ideal wiggler.

We now consider the characteristics of particle trajectories which are close to these steady-state trajectories. To this end we write $v_1 = v_w + \delta v_1$, $v_2 = \delta v_2$, $v_3 = v_{||} + \delta v_3$, $\chi = \pm\pi/2 + \delta\chi$, and $\lambda = \mp v_w/v_{||} + \delta\lambda$. To first order in the perturbed quantities, therefore, we find that Eq. (3) implies

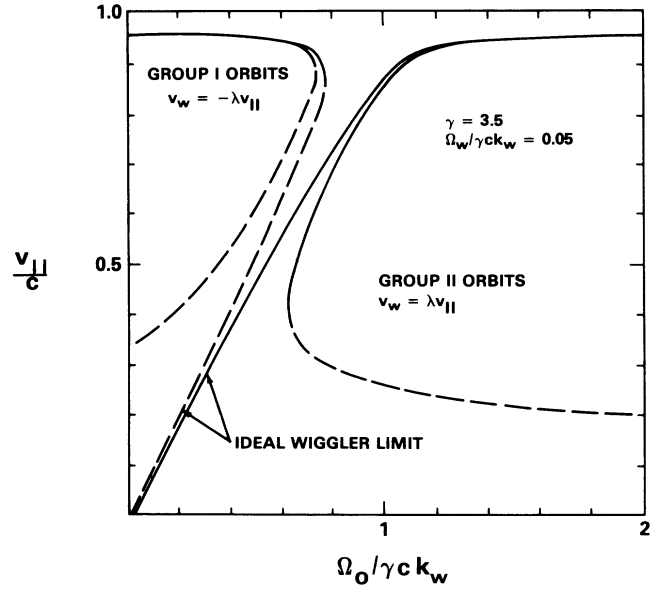


FIG. 1. Graph of the axial velocity of the steady-state orbits vs guide-field strength for ideal and realizable wiggler models.

$$\begin{aligned}\gamma\delta\dot{v}_1 &= -[\Omega_0 - \gamma k_w v_{||} \pm 2\Omega_w I_1(\lambda_0)]\delta v_2 - 2\Omega_w v_{||} I_2(\lambda_0)\delta\chi, \\ \gamma\delta\dot{v}_2 &= [\Omega_0 - \gamma k_w v_{||} \pm 2\Omega_w I_1(\lambda_0)]\delta v_1 \\ &\quad - [\gamma k_w v_w + 2\Omega_w I_1(\lambda_0)]\delta v_3 \\ &\quad - 2\Omega_w v_{||} \lambda_0^{-1} \delta\lambda [I_2(\lambda_0) + \lambda_0^2 I_0(\lambda_0) - \lambda_0 I_1(\lambda_0)], \\ \gamma\delta\dot{v}_3 &= 2\Omega_w v_w I_2(\lambda_0)\delta\chi + 2\lambda_0^{-1} \Omega_w I_1(\lambda_0)\delta v_2, \quad (6) \\ \delta\dot{\chi} &= -k_w (\delta v_3 \pm \lambda_0^{-1} \delta v_1 \mp \lambda_0^{-2} v_w \delta\lambda), \\ \delta\dot{\lambda} &= \pm k_w (\delta v_2 - v_w \delta\chi),\end{aligned}$$

where we denote $\lambda_0 \equiv \mp v_w/v_{||}$. The system of first-order differential equations represented by (6) can be simplified to a pair of fourth-order equations

$$\left[\frac{d^2}{dt^2} + \Omega_1^2 \right] \left[\frac{d^2}{dt^2} + \Omega_2^2 \right] \begin{bmatrix} \delta v_2 \\ \delta\chi \end{bmatrix} = 0, \quad (7)$$

where

$$\Omega_{1,2}^2 \equiv \frac{1}{2} (\omega_1^2 + \omega_2^2) \pm \frac{1}{2} [(\omega_1^2 - \omega_2^2)^2 + 4A_2 B_2]^{1/2}, \quad (8)$$

and

$$\begin{aligned}\omega_1^2 &\equiv k_w^2 v_{||}^2 \mp 2\gamma^{-1} \Omega_w k_w v_{||} \lambda_0^{-1} (1 + \lambda_0^2) I_2(\lambda_0), \\ \omega_2^2 &\equiv \gamma^{-2} (\Omega_0 - \gamma k_w v_{||}) [\Omega_0 \pm 2\Omega_w I_1(\lambda_0) - \gamma k_w v_{||}] \\ &\quad \pm 2\gamma^{-1} \Omega_w k_w v_{||} \lambda_0^{-1} (1 + \lambda_0^2) I_2(\lambda_0), \\ A_2 &\equiv \pm c k_w \lambda_0^{-1} \gamma^{-1} (\Omega_0 - 2\gamma k_w v_{||}), \\ B_2 &\equiv -2\gamma^{-2} \Omega_w \beta_{||} \{ (1 + \lambda_0^2) [\Omega_0 \pm 2\Omega_w I_1(\lambda_0)] I_2(\lambda_0) \\ &\quad + \lambda_0^2 \gamma k_w v_{||} [I_0(\lambda_0) - \lambda_0^{-1} I_1(\lambda_0)] \},\end{aligned}$$

and $\beta_{||} \equiv v_{||}/c$. Observe that Ω_1^2 and Ω_2^2 must be computed separately for each class of steady-state orbit, and that an orbital instability occurs whenever either Ω_1^2 or Ω_2^2 becomes negative. These frequencies are plotted in Fig. 2

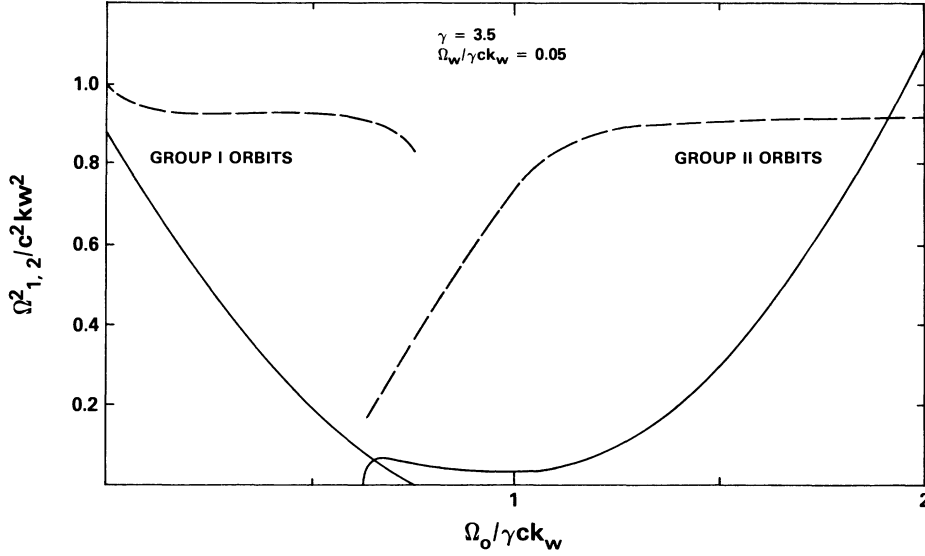


FIG. 2. Graphs of $\Omega_1^2/c^2k_w^2$ (dashed line) and $\Omega_2^2/c^2k_w^2$ (solid line) vs $\Omega_0/\gamma ck_w$ for group I and group II orbits.

versus β_0 (for $\beta_w=0.05$ and $\gamma=3.5$) for stable trajectories (i.e., $\Omega_1^2, \Omega_2^2 > 0$). Note that the unstable trajectories are represented in Fig. 1 by the dashed lines. It is evident from Fig. 2 that $\Omega_1^2 \gg \Omega_2^2$ and $\Omega_1 \sim k_w v_{||}$ except for a narrow range of axial fields corresponding to group II orbits in the neighborhood of $\Omega_0 \sim \gamma k_w v_{||}$. Also, Ω_2^2 varies widely and the orbital instability occurs when $\Omega_2^2 < 0$.

The solutions to Eq. (7) are of the form

$$\delta v_2 = -\alpha_1 \sin(\Omega_1 t - \phi_1) - \alpha_2 \sin(\Omega_2 t - \phi_2)$$

and

$$\delta \chi = -\rho_1 \sin(\Omega_1 t - \theta_1) - \rho_2 \sin(\Omega_2 t - \theta_2),$$

where $\alpha_1, \alpha_2, \rho_1, \rho_2, \phi_1, \phi_2, \theta_1,$ and θ_2 are the integration constants. Using these solutions we can derive the appropriate forms for δv_1 and δv_3 from Eqs. (6). However, we note that since $\Omega_1 \lesssim k_w v_{||}$, such terms will provide for interactions at higher harmonics of the free-electron-laser Doppler upshift. Thus, since we confine ourselves to treatment of the interaction at the fundamental Doppler upshift, we are justified in neglecting oscillatory terms in Ω_1 (which is equivalent to the requirement that $\alpha_1 = \rho_1 = 0$). Within this context, the other components of

the velocity are

$$\delta v_1 = -\frac{2\Omega_w}{\Omega_2} [\mp \lambda_0^{-2} I_1(\lambda_0) \alpha_2 \cos(\Omega_2 t - \phi_2) + \rho_2 v_{||} I_2(\lambda_0) \cos(\Omega_2 t - \phi_2)] \quad (9)$$

and

$$\delta v_3 = \lambda_0 \frac{2\Omega_w}{\Omega_2} [\lambda_0^{-2} I_1(\lambda_0) \alpha_2 \cos(\Omega_2 t - \phi_2) \mp \rho_2 v_{||} I_2(\lambda_0) \cos(\Omega_2 t - \phi_2)]. \quad (10)$$

Observe that $\delta v_1 \mp \lambda_0 \delta v_{||} = \text{const.}$ The further constraint imposed by energy conservation implies that $\theta_2 = \phi_2$, and

$$\alpha_2^2 = \frac{4\Omega_w^2}{\Omega_2^2} (1 + \lambda_0^2) \left[\mp \frac{\alpha_2}{\lambda_0^2} I_1(\lambda_0) + v_{||} \rho_2 I_2(\lambda_0) \right]^2. \quad (11)$$

As a consequence, the orbits can be written in the following form in rectangular coordinates:

$$\begin{aligned} p_x &= p_w \cos k_w z + (1 + \lambda^2)^{-1/2} \alpha_+ [P_x \cos(k_w z - \Omega_2 t) - P_y \sin(k_w z - \Omega_2 t)] \\ &\quad + (1 + \lambda^2)^{-1/2} \alpha_- [P_x \cos(k_w z + \Omega_2 t) + P_y \sin(k_w z + \Omega_2 t)], \\ p_y &= p_w \sin k_w z + (1 + \lambda^2)^{-1/2} \alpha_+ [P_x \sin(k_w z - \Omega_2 t) + P_y \cos(k_w z - \Omega_2 t)] \\ &\quad + (1 + \lambda^2)^{-1/2} \alpha_- [P_x \sin(k_w z + \Omega_2 t) - P_y \cos(k_w z + \Omega_2 t)], \\ p_z &= p_{||} - \frac{P_w}{p_{||}} (1 + \lambda_0^2)^{-1/2} (P_x \cos \Omega_2 t + P_y \sin \Omega_2 t), \end{aligned} \quad (12)$$

where $\alpha_{\pm} \equiv [1 \pm (1 + \lambda_0^2)^{1/2}]/2$, $p_w \equiv \gamma m v_w$, $p_{||} \equiv \gamma m v_{||}$, $P_x \equiv \gamma m \alpha_2 \cos \phi_2$, and $P_y \equiv \gamma m \alpha_2 \sin \phi_2$ are analogs of the canonical momenta. Observe that $\lim_{\lambda_0 \rightarrow 0} \Omega_2 = k_w v_{||} - \Omega_0/\gamma$, $\lim_{\lambda_0 \rightarrow 0} \alpha_+ = 1$, and $\lim_{\lambda_0 \rightarrow 0} \alpha_- = 0$; hence, (12) reduces to the orbit equations used by Freund *et al.*¹⁶ in the one-dimensional limit and (P_x, P_y) are the usual canonical momenta in the limit $B_0 \rightarrow 0$.

Before closing this section, some discussion is in order in regard to the transition to orbital instability at $\Omega_2=0$. The gain exhibits large enhancements in this region since the natural response frequency of electron motion (Ω_2 in the wiggler frame) is small and can be comparable to the frequency of the ponderomotive wave which drives the stimulated radiation process in free-electron lasers. For simplicity, we consider the product $\Omega_1^2\Omega_2^2$ rather than Ω_2^2 independently (since $\Omega_1 \sim k_w v_{||}$ this cannot affect the orbital instability criterion), and find that

$$\{(1+\lambda_0^2)[\Omega_0 \pm 2\Omega_w I_1(\lambda_0)] - \gamma k_w v_{||}\} Z(\lambda_0) - \gamma \lambda_0^2 k_w v_{||} Y(\lambda_0) = 0 \quad (13)$$

at the transition to orbital instability, where

$$Z(\lambda_0) \equiv (1+\lambda_0^2)I_1'(\lambda_0) - \frac{2}{\lambda_2} I_1(\lambda_0) \quad (14)$$

and

$$Y(\lambda_0) \equiv (1+\lambda_0^2)I_1'(\lambda_0) - \frac{1}{\lambda_0} I_1(\lambda_0). \quad (15)$$

In the limit in which $\lambda_0 \ll 1$ and $B_w \ll B_0$, Eq. (13) reduces to $(1+\lambda_0^2)\Omega_0 - \gamma k_w v_{||} = 0$, which is the orbital instability threshold found using an idealized one-dimensional wiggler field.^{16,20}

III. THE SOURCE CURRENT AND CHARGE DENSITY

The source current and charge density are obtained from the moments of the perturbed distribution function

$$\delta f_b(\vec{r}(z), z, \vec{p}, \tau(z)) = e \int_0^z \frac{dz'}{v_z(\vec{r}(z'), z')} \left[\delta \vec{E}(\vec{r}(z'), z', \tau(z')) + \frac{1}{c} \vec{v}(\vec{r}(z'), z') \times \delta \vec{B}(\vec{r}(z'), z', \tau(z')) \right] \cdot \frac{\partial F_b}{\partial \vec{p}'}, \quad (16)$$

where F_b is the equilibrium distribution, $\delta \vec{E}$ and $\delta \vec{B}$ are the fluctuating electromagnetic fields, $\vec{r}(z')$ is the position of the electron relative to the axis of symmetry at z' , $\tau(z') = t_0 + \int_0^z dz'/v_z(\vec{r}(z'), z')$ is the sum of the time required for an electron to travel from $(\vec{r}(z=0), z=0)$ at the start of the interaction region to $(\vec{r}(z=z'), z=z')$ and the entry time t_0 . The equilibrium distribution must be a function of the constants of the motion (P_x, P_y, p) , where small P_x and P_y are required. As a consequence, we choose a distribution of the form

$$F_b(P_x, P_y, p) = n_b \delta(P_x) \delta(P_y) G_b(p), \quad (17)$$

where n_b is the average beam density, and $G_b(p)$ is an arbitrary function of the total momentum. In addition, we work with vector and scalar potentials of the form

$$(\delta \vec{A}(\vec{x}, t), \delta \phi(\vec{x}, t)) = \frac{1}{2} (\delta \hat{A}(\vec{x}), \delta \hat{\phi}(\vec{x})) \exp(-i\omega t) + c.c. \quad (18)$$

With respect to the basis $\hat{e}_{\pm} = \frac{1}{2}(\hat{e}_x \mp i\hat{e}_y)$, integration of (16) yields

$$\delta \hat{f}_b(\vec{r}(z), z) = \left[D_+ \left[\frac{\partial}{\partial P_x} - i \frac{\partial}{\partial P_y} \right] + D_- \left[\frac{\partial}{\partial P_x} + i \frac{\partial}{\partial P_y} \right] + D_z \frac{\partial}{\partial p} \right] F_b(P_x, P_y, p), \quad (19)$$

where

$$D_z \equiv \frac{e}{2cp} \int_0^z dz' \frac{e^{i\omega\tau(z, z')}}{v_z(\vec{r}(z'), z')} \left[-c(p_z \nabla_z + \frac{1}{2}p_- \nabla_+ + \frac{1}{2}p_+ \nabla_-) \delta \hat{\phi} + i\omega(p_z \delta \hat{A}_z + p_- \delta \hat{A}_+ + p_+ \delta \hat{A}_-) \right], \quad (20)$$

$$D_{\pm} \equiv \frac{e}{2c} \int_0^z dz' \frac{e^{i\omega\tau(z, z')}}{v_z(\vec{r}(z'), z')} \left[\alpha_+ e^{\mp i\theta_-} \left[-\frac{c}{2} \nabla_{\mp} \delta \hat{\phi} + (i\omega - v_z \nabla_z) \delta \hat{A}_{\mp} + \frac{1}{2} v_z \nabla_{\mp} \delta \hat{A}_z \pm \frac{v_{\mp}}{2} (\nabla_- \delta \hat{A}_+ - \nabla_+ \delta \hat{A}_-) \right] \right. \\ \left. - \alpha_- e^{\pm i\theta_+} \left[-\frac{c}{2} \nabla_{\pm} \delta \hat{\phi} + (i\omega - v_z \nabla_z) \delta \hat{A}_{\pm} + \frac{1}{2} v_z \nabla_{\pm} \delta \hat{A}_z \mp \frac{v_{\pm}}{2} (\nabla_- \delta \hat{A}_+ - \nabla_+ \delta \hat{A}_-) \right] \right], \quad (21)$$

where $\tau(z, z') \equiv \tau(z) - \tau(z')$, $p_{\pm} \equiv p_x \mp ip_y$, $\delta \hat{A}_{\pm} \equiv \delta \hat{A}_x \mp i \delta \hat{A}_y$, $\nabla_{\pm} \equiv \partial_x \mp i \partial_y$, $\nabla_z \equiv \partial_z$, and $\theta_{\pm} \equiv k_w z \pm \Omega_2 \tau(z)$.

The current and charge density are found by computation of the appropriate moments of (19) as

$$\delta \hat{J}_{\pm} = -\frac{e}{m} \int dP_x dP_y dp (1+\lambda^2)^{-1/2} \frac{p p_{\pm}}{\gamma p_z} \delta \hat{f}_{\pm}, \quad \delta \hat{J}_z = -\frac{e}{m} \int dP_x dP_y dp (1+\lambda^2)^{-1/2} \frac{p}{\gamma} \delta \hat{f}, \quad (22)$$

and

$$\delta\hat{\rho} = -e \int dP_x dP_y dp (1 + \lambda^2)^{-1/2} \frac{p}{p_z} \delta\hat{f}. \quad (23)$$

By application of Floquet's theorem, we express the axial and azimuthal structure of the fields and sources in the form

$$\delta\hat{f}(\vec{r}, z) = \sum_{l, n = -\infty}^{\infty} \delta\hat{f}_{l, n}(r) \exp[i(k + nk_w)z + il\theta], \quad (24)$$

in cylindrical coordinates. As might be expected, substitution of (19) into (22) and (23) results in source currents $\delta\hat{J}_{l, n}$ and charge densities $\delta\hat{\rho}_{l, n}$, each of which depends upon a complicated superposition of many harmonics of $\delta\hat{A}_{l, n}$ and $\delta\hat{\phi}_{l, n}$. However, in the limit in which the frequency $\omega \gg \Omega_2$, $\partial | \delta\hat{A}_{l, n}(r) | / \partial r \ll k$, and $\partial | \delta\hat{\phi}_{l, n}(r) | / \partial r \ll k$ we find the comparatively simple forms

$$\delta\hat{J}_{l, n}^{(\pm)} \simeq -\frac{i\omega_b^2}{8\pi c} \int_0^\infty dp \frac{1}{\gamma} \left[[p_\omega (\hat{H}_{l, n}^{\pm} + \hat{H}_{l \mp 2, n \pm 2}^{\mp}) - ip_{||} (ck_{n \pm 1} \delta\hat{\phi}_{l \mp 1, n \pm 1} - \omega \delta\hat{A}_{l \mp 1, n \pm 1, z})] \frac{p_\omega}{\omega - k_{n+1} v_{||}} \frac{1}{p} \frac{\partial}{\partial p} - \frac{2\alpha_{\pm}^2}{\omega \pm \Omega_2 - k_{n+1} v_{||}} \hat{L}_{l, n}^{(\pm) \mp} \lambda^2 (1 + \lambda^2)^{-1/2} \frac{\omega}{\Omega_2} (R_{l, n}^{(\pm)} \hat{L}_{l, n}^{(\pm)} - R_{l, n}^{(\mp)} \hat{L}_{l \mp 2, n \pm 2}^{(\mp)}) \right] G_b(p) \quad (25)$$

and

$$\delta\hat{\rho}_{l, n} \simeq -\frac{i\omega_b^2}{8\pi c} \int_0^\infty dp \frac{1}{\gamma v_w} \left[[p_\omega (\hat{H}_{l-1, n+1}^{(-)} + \hat{H}_{l+1, n-1}^{(+)}) - ip_{||} (ck_n \delta\hat{\phi}_{l, n} - \omega \delta\hat{A}_{l, n, z})] \frac{p_\omega}{\omega - k_{n+1} v_{||}} \frac{1}{p} \frac{\partial}{\partial p} + \lambda^2 (1 + \lambda^2)^{-1/2} \frac{\omega}{\Omega_2} (\hat{L}_{l-1, n+1}^{(-)} R_{l, n}^{(-)} - \hat{L}_{l+1, n-1}^{(+)} R_{l, n}^{(+)} + \frac{1}{2} v_w \hat{K}_{l, n} S_{l, n}) \right] G_b(p), \quad (26)$$

where $\delta\hat{J}_{l, n}^{(\pm)} \equiv (\delta\hat{J}_{l, n})_r \mp i(\delta\hat{J}_{l, n})_\theta$, $\delta\hat{A}_{l, n}^{(\pm)} \equiv \frac{1}{2} [(\delta\hat{A}_{l, n})_r \mp i(\delta\hat{A}_{l, n})_\theta]$, $\omega_b^2 \equiv 4\pi e^2 n_b / m$ is the average plasma frequency, $\nabla_l^{(\pm)} \equiv \partial / \partial r \pm l / r$,

$$\begin{aligned} \hat{L}_{l, n}^{(\pm)} &\equiv i(\omega - k_n v_{||}) \delta\hat{A}_{l, n}^{(\pm)} - \frac{1}{2} \nabla_l^{(\pm)} (c \delta\hat{\phi}_{l, n} - v_{||} \delta\hat{A}_{l, n, z}), \\ \hat{H}_{l, n}^{(\pm)} &\equiv i\omega \delta\hat{A}_{l, n}^{(\pm)} - \frac{1}{2} c \nabla_l^{(\pm)} \delta\hat{\phi}_{l, n}, \quad \hat{K}_{l, n} \equiv \nabla_{l-1}^{(-)} \delta\hat{A}_{l, n}^{(+)} - \nabla_{l+1}^{(+)} \delta\hat{A}_{l, n}^{(-)}, \\ R_{l, n}^{(\pm)} &\equiv \frac{\alpha_+}{\omega \pm \Omega_2 - k_{n+1} v_{||}} + \frac{\alpha_-}{\omega \mp \Omega_2 - k_{n+1} v_{||}} - \frac{1}{\omega - k_{n+1} v_{||}}, \end{aligned} \quad (27)$$

and

$$S_{l, n} \equiv \frac{1}{\omega - \Omega_2 - k_{n+1} v_{||}} + \frac{1}{\omega + \Omega_2 - k_{n+1} v_{||}} - \frac{2}{\omega - k_{n+1} v_{||}}. \quad (28)$$

Observe that $\delta\hat{J}_{l, n, z}$ has been omitted because the specification of a gauge condition allows us to eliminate one of the components ($\delta\hat{A}, \delta\hat{\phi}$), and we choose to deal with $\delta\hat{A}_{\pm}$ and $\delta\hat{\phi}$.

It should also be remarked that our choice of distribution (17) is equivalent to the requirement that the unperturbed orbits are of the steady-state type ($P_x = P_y = 0$). Such orbits are axicentered, and there is a unique mapping between the radius of the orbit and the particle energy (for given B_w, B_0 , and λ_w). As a consequence, a small spread in the energy of the beam will imply a narrow radial profile.

IV. THE MAXWELL-POISSON EQUATIONS

The starting point for the development in this section is the Maxwell-Poisson equations

$$\left[\frac{1}{r} \frac{d}{dr} r \frac{d}{dr} + p_n^2 - \frac{(l \mp 1)^2}{r^2} \right] \delta\hat{A}_{l, n}^{(\pm)} = -\frac{4\pi}{c} \delta\hat{J}_{l, n}^{(\pm)}, \quad (29)$$

$$\left[\frac{1}{r} \frac{d}{dr} r \frac{d}{dr} + p_n^2 - \frac{l^2}{r^2} \right] \delta\hat{\phi}_{l, n} = -8\pi \delta\hat{\rho}_{l, n}, \quad (30)$$

as well as the Lorentz gauge condition

$$k_n \delta\hat{A}_{l, n, z} = \frac{\omega}{c} \delta\hat{\phi}_{l, n} + i(\nabla_{l-1}^{(-)} \delta\hat{A}_{l, n}^{(+)} + \nabla_{l+1}^{(+)} \delta\hat{A}_{l, n}^{(-)}), \quad (31)$$

where $p_n^2 \equiv \omega^2/c^2 - k_n^2$. In order to carry the analysis further, a distribution function must be specified in order to evaluate the sources. We choose $G_b(p) = N(p)\delta[p - p(r)]$, where $p(r)$ is the mapping between the energy and the radius of the steady-state trajectory

$$p(r) = mc(1 + \lambda^2)^{1/2} [\gamma\beta_0 \pm 2\gamma\beta_w \lambda^{-2}(1 + \lambda^2)I_1(\lambda)], \quad (32)$$

$N(p)$ is an arbitrary function of p which is chosen such that $N(p(r))$ models the density profile, and $\omega_b^2(r) \equiv 4\pi e^2 n_0 N(p(r))/m$ is the local plasma frequency. As a consequence, by retaining only the dominant coupling terms, we find

$$\delta\hat{J}_{l,n}^{(\pm)} \simeq \frac{c}{4\pi} (\Lambda_{l,n}^{(\pm)} \delta\hat{A}_{l,n}^{(\pm)} + T_{l\mp 1, n\pm 1} \delta\hat{\phi}_{l\mp 1, n\pm 1} + V_{l\mp 2, n\pm 2} \delta\hat{A}_{l\mp 2, n\pm 2}^{(\mp)}) \quad (33)$$

and

$$\delta\hat{\rho}_{l,n} \simeq \frac{1}{4\pi} (\chi_{l,n} \delta\hat{\phi}_{l,n} + W_{l+1, n-1} \delta\hat{A}_{l+1, n-1}^{(+)} + W_{l-1, n+1} \delta\hat{A}_{l-1, n+1}^{(-)}), \quad (34)$$

where

$$\Lambda_{l\pm 1, n\mp 1}^{(\pm)} \equiv -\frac{\omega_b^2(r)}{\gamma c^2} \left[\omega - k_n v_{||} \left[1 + \frac{l^2}{2k_n^2 r^2} \right] \right] \left[\frac{\alpha_+^2}{\omega \pm \Omega_2 - k_{n+l} v_{||}} + \frac{\alpha_-^2}{\omega \mp \Omega_2 - k_{n+l} v_{||}} \right] + V_{l\pm 1, n\mp 1}, \quad (35)$$

$$\chi_{l,n} \equiv -\frac{\omega_b^2(r)}{\gamma c^2} \frac{\omega^2 - c^2 k_n^2}{v_{||} k_n} \frac{k_{n+l} v_{||}}{\gamma^2 (1 + \lambda^2) (\omega - k_{n+l} v_{||})^2} \left[1 + \lambda^2 Q(\lambda) \frac{\omega}{k_{n+l} v_{||}} \right], \quad (36)$$

$$T_{l,n}^{(\pm)} \equiv -\frac{\omega_b^2(r)}{2\gamma c^2} \frac{p_w}{p_{||}} \frac{\omega^2 - c^2 k_n^2}{ck_n} \frac{\omega}{\gamma^2 (1 + \lambda^2) (\omega - k_{n+l} v_{||})^2} \left[1 - Q(\lambda) \frac{(1 - \lambda^2)\omega - k_{n+l} v_{||}}{\omega} \right], \quad (37)$$

$$W_{l\pm 1, n\mp 1} \equiv -\frac{\omega_b^2(r)}{\gamma c^2} \frac{p_w}{p_{||}} \frac{\omega k_{n+l} c}{\gamma^2 (1 + \lambda^2) (\omega - k_{n+l} v_{||})^2} \left[1 - Q(\lambda) \frac{\omega - (1 + \lambda^2) k_{n+l} v_{||}}{k_{n+l} v_{||}} \right], \quad (38)$$

$$V_{l\pm 1, n\mp 1} \equiv -\frac{\omega_b^2(r)}{2\gamma c^2} \frac{\lambda^2 \omega^2}{\gamma^2 (1 + \lambda^2) (\omega - k_{n+l} v_{||})^2} \left[1 - Q(\lambda) \frac{2(\omega - k_{n+l} v_{||}) - \lambda^2 k_{n+l} v_{||}}{\omega} \right]. \quad (39)$$

In Eqs. (35)–(39) ($\gamma, v_{||}, v_w$) are implicit functions of r and

$$Q(\lambda) \equiv \frac{\gamma^3 k_w v_{||} I_1(\lambda)/\lambda}{\{(1 + \lambda^2)[\Omega_0 \pm 2\Omega_w I_1(\lambda)] - \gamma k_w v_{||}\} Z(\lambda) - \lambda^2 \gamma k_w v_{||} Y(\lambda)}, \quad (40)$$

which contains a singularity at the transition to orbital instability for the group I and group II orbits. In the vicinity of these points, therefore, we expect the interaction strength to be greatly enhanced. Analogous results were found in the idealized one-dimensional theory.^{16,20} As a consequence, we obtain the following set of coupled differential equations:

$$\left[\frac{1}{r} \frac{d}{dr} r \frac{d}{dr} + p_{n\mp 1}^2 - \frac{l^2}{r^2} \right] \delta\hat{A}_{l\pm 1, n\mp 1}^{(\pm)} = -\Lambda_{l\pm 1, n\mp 1}^{(\pm)} \delta\hat{A}_{l\pm 1, n\mp 1}^{(\pm)} - T_{l,n}^{(\pm)} \delta\hat{\phi}_{l,n} - V_{l\mp 1, n\pm 1} \delta\hat{A}_{l\mp 1, n\pm 1}^{(\mp)}, \quad (41)$$

$$\left[\frac{1}{r} \frac{d}{dr} r \frac{d}{dr} + p_n^2 - \frac{l^2}{r^2} \right] \delta\hat{\phi}_{l,n} = -\chi_{l,n} \delta\hat{\phi}_{l,n} - W_{l+1, n-1} \delta\hat{A}_{l+1, n-1}^{(+)} - W_{l-1, n+1} \delta\hat{A}_{l-1, n+1}^{(-)}. \quad (42)$$

In order to solve this set of differential equations, we must specify the boundary conditions appropriate to a cylindrical waveguide of radius R_g . We assume the walls to be grounded and at zero potential; hence,

$$\begin{aligned} \delta\hat{\phi}_{l,n}(R_g) &= \delta\hat{A}_{l,n}^{(\pm)}(R_g) \\ &= \frac{d}{dr} [r(\delta\hat{A}_{l,n}^{(+)} + \delta\hat{A}_{l,n}^{(-)})] |_{r=R_g} = 0. \end{aligned} \quad (43)$$

It should be observed that Eqs. (41)–(43) describe a coupling between five harmonic components: $\delta\hat{\phi}_{l,n}$, $\delta\hat{A}_{l+1, n-1}^{(\pm)}$, and $\delta\hat{A}_{l-1, n+1}^{(\pm)}$. Finally, we also assume that the potentials are continuous within the waveguide (i.e.,

across the boundary of the electron beam). The problem, therefore, has been specified with the essential physics of the interaction contained within the radial dependence of the coupling coefficients in (41) and (42). It is important to observe that with the above choice of indices, the azimuthal mode number for the electromagnetic waveguide modes is given by $l \pm 1$, and not simply by l . Thus, if we wish to study the TE_{lm} or TM_{lm} modes for the $\delta\hat{A}_{l\pm 1, n\pm 1}^{(\pm)}$ eigenvector, then we must set $l=0$.

V. THE LIMIT OF A THIN BEAM

A solution to Eqs. (41)–(43) is found for the case of a thin beam in which the density profile is assumed to be

constant (n_0) within the range $R_0 - \Delta R \leq r \leq R_0$. As a result, in the limit in which $\Delta R \ll R_0$ the beam density is given approximately by

$$n_b(r) = n_0 \Delta R \delta(r - R_0). \tag{44}$$

It should be remarked that we have assumed the unperturbed orbits to be the stable steady-state trajectories. These orbits are axicentered and, for orbits of either group I or group II, there is a unique mapping between γ and λ (i.e., the orbit radius) for given B_0 , B_w , and λ_w . Thus, it is sufficient to specify the class of orbit and $R_0(\gamma_0)$ in order to obtain $\gamma_0(R_0)$. In addition, a spread in radius ΔR of the beam is equivalent to an energy spread $\Delta\gamma$ given by

$$\frac{\Delta\gamma}{\gamma_0} = \frac{\gamma_0^2 - 1}{(1 + \lambda_0^2)Q(\lambda_0)} \frac{\Delta R}{R_0}, \tag{45}$$

where $\lambda_0 \equiv k_w R_0$. Observe that within the context of our analysis, a thin beam is equivalent to a relatively small energy spread.

The solutions are of the form

$$\delta\phi_{l,n} = A_{l,n} J_l(p_n r), \quad \delta A_{l,n}^{(\pm)} = A_{l,n}^{\pm} J_{l\mp 1}(p_n r), \tag{46}$$

for $0 \leq r < R_0$, and

$$\delta\phi_{l,n} = B_{l,n} J_l(p_n r) + C_{l,n} N_l(p_n r), \tag{47}$$

$$\delta A_{l,n}^{(\pm)} = B_{l,n}^{\pm} J_{l\mp 1}(p_n r) + C_{l,n}^{\pm} N_{l\mp 1}(p_n r)$$

for $r > R_0$. In (46) and (47) $J_l(x)$ and $N_l(x)$ are the regular Bessel functions of the first and second kind of order l . Observe that each field quantity (i.e., $\delta\phi_{l,n}$, $\delta A_{l+1,n-1}^{(+)}$, $\delta A_{l-1,n+1}^{(-)}$, $\delta A_{l-1,n+1}^{(+)}$, and $\delta A_{l+1,n-1}^{(-)}$) requires three coefficients to characterize the solution throughout the waveguide. Two of these coefficients may be determined from the boundary conditions at $r = R_0$, and R_g . The third coefficient is found by multiplying the field equations by r and integrating over $R_0 - \epsilon \leq r \leq R_0 + \epsilon$ in the limit $\epsilon \rightarrow 0^+$. This procedure determines the ‘‘jump condition’’ across the thin beam, and allows us to obtain a 5×5 matrix equation in, for example, the coefficients $A_{l,n}$, $A_{l+1,n-1}^+$, $A_{l-1,n+1}^-$, $A_{l-1,n+1}^+$, and $A_{l+1,n-1}^-$. Observe that the coupling to the field components in $\delta A_{l\mp 1,n\pm 1}^{(\pm)}$ occurs not through the source terms in the field equations but rather through the boundary condition at the waveguide wall.

The matrix equation obtained in this manner can be written as

$$\begin{pmatrix} \epsilon_{l,n} & -\frac{\pi}{2} R_0 \Delta R \bar{W}_{l+1,n-1} & -\frac{\pi}{2} R_0 \Delta R \bar{W}_{l-1,n+1} \\ \frac{\pi}{2} R_0 \Delta R \bar{T}_{l,n} & \epsilon_{l+1,n-1}^{(+)} & \frac{\pi}{2} R_0 \Delta R \bar{V}_{l-1,n+1} \\ \frac{\pi}{2} R_0 \Delta R \bar{T}_{l,n} & \frac{\pi}{2} R_0 \Delta R \bar{V}_{l+1,n-1} & \epsilon_{l-1,n+1}^{(-)} \end{pmatrix} \begin{pmatrix} A_{l,n} \\ A_{l+1,n-1}^{(+)} \\ A_{l-1,n+1}^{(-)} \end{pmatrix} = 0, \tag{48}$$

where the equations for $A_{l-1,n+1}^{(+)}$ and $A_{l+1,n-1}^{(-)}$ have already been eliminated,

$$\epsilon_{l,n} \equiv D_{l,n} - \frac{\pi}{2} R_0 \Delta R \bar{\chi}_{l,n}, \tag{49}$$

$$\begin{aligned} \epsilon_{l\pm 1,n\mp 1}^{(\pm)} &\equiv D_{l\pm 1,n\mp 1}^{(\pm)} \\ &+ \frac{\pi}{2} R_0 \Delta R (\bar{\Lambda}_{l\pm 1,n\mp 1}^{(\pm)} + \bar{\Lambda}_{l\pm 1,n\mp 1}^{(\mp)} M_{l\mp 1,n\pm 1}^{(l\pm 2)}), \end{aligned} \tag{50}$$

where $\bar{W}_{l\pm 1,n\mp 1}$, $\bar{V}_{l\pm 1,n\mp 1}$, $\bar{\Lambda}_{l\pm 1,n\mp 1}^{(\pm)}$, $\bar{T}_{l,n}$, and $\bar{\chi}_{l,n}$ denote those quantities specified in Eqs. (35)–(39) in which the substitution $\omega_b^2(r) = 4\pi e^2 n_0 / m$ has been made. In addition,

$$D_{l,n} \equiv \frac{J_l(\xi_n)}{J_l(\xi_n)[J_l(\xi_n)N_l(\xi_n) - J_l(\xi_n)N_l(\xi_n)]}, \tag{51}$$

$$D_{l\pm 1,n\mp 1}^{(\pm)} \equiv \frac{2J_{l\pm 1}(\xi_{n\mp 1})J'_{l\pm 1}(\xi_{n\mp 1})}{J_l(\xi_{n\mp 1})S_{l\pm 1,n\mp 1}^{(l\pm 2)}}, \tag{52}$$

and

$$M_{l\mp 1,n\pm 1}^{(l\pm 2)} \equiv \frac{J_{l\pm 2}(\xi_{n\mp 1})\Gamma_{l\pm 1,n\mp 1}^{(l\pm 2)}}{J_l(\xi_{n\mp 1})S_{l\pm 1,n\mp 1}^{(l\pm 2)}}, \tag{53}$$

where $\xi_n \equiv p_n R_0$, $\xi_n \equiv p_n R_g$, and J'_l is the derivative of the Bessel function. In (52) and (53),

$$\begin{aligned} \Gamma_{k,m}^{(l)} &\equiv N_l(\xi_m) \frac{d}{d\xi_m} J_k^2(\xi_m) \\ &- J_l(\xi_m) \frac{d}{d\xi_m} [N_k(\xi_m)J_k(\xi_m)], \end{aligned} \tag{54}$$

$$S_{k,m}^{(l\pm 2)} \equiv \Gamma_{k,m}^{(l)} + \frac{\pi}{2} R_0 \Delta R \bar{\Lambda}_{k,m}^{\mp} J_{l\pm 2}(\xi_m) \Psi_{k,m}^{(l\pm 2)}, \tag{55}$$

and

$$\begin{aligned} \Psi_{k,m}^{(l\pm 2)} &\equiv N_{l\pm 2}(\xi_m) \Gamma_{k,m}^{(l)} \\ &- J_{l\pm 2}(\xi_m) \left[N_l(\xi_m) \frac{d}{d\xi_m} [N_k(\xi_m)J_k(\xi_m)] \right. \\ &\quad \left. - J_l(\xi_m) \frac{d}{d\xi_m} N_k^2(\xi_m) \right]. \end{aligned} \tag{56}$$

The dispersion equation is found by setting the determinant of this interaction matrix to zero.

Substantial simplification occurs in the limit in which $|\omega - k_{n+1}v_{||}| \ll \omega$, $|k_{n+1}v_{||}|$ and we obtain

$$\bar{\chi}_{l,n} \simeq -\frac{\omega_b^2}{\gamma_0 c^2} \frac{c}{v_{\parallel}} \frac{\omega^2 - c^2 k_n^2}{ck_n} \frac{\omega}{\gamma_0^2 (1 + \lambda_0^2) (\omega - k_{n+l} v_{\parallel})^2} \Phi, \quad \bar{V}_{l,\pm 1, n \mp 1} \simeq \frac{1}{2} \frac{v_w}{c} \bar{W}_{l,\pm 1, n \mp 1}, \quad (57)$$

$$\bar{W}_{l,\pm 1, n \mp 1} \simeq -\frac{v_w}{v_{\parallel}} \frac{\omega_b^2}{\gamma_0 c^2} \frac{c}{v_{\parallel}} \frac{\omega^2}{\gamma_0^2 (1 + \lambda_0^2) (\omega - k_{n+l} v_{\parallel})^2} \Phi, \quad \bar{T}_{l,n} \simeq \frac{1}{2} \frac{v_w}{c} \bar{\chi}_{l,n}, \quad (58) \quad \text{and}$$

$$\bar{\Lambda}_{l,\pm 1, n \mp 1}^{(\pm)} \simeq -\lambda_0^2 \frac{\omega_b^2}{2\gamma_0 c^2} \frac{\omega^2}{\gamma_0^2 (1 + \lambda_0^2) (\omega - k_{n+l} v_{\parallel})^2} \Phi - \frac{\omega_b^2}{\gamma_0 c^2} \left[\omega - k_{n+l} v_{\parallel} \left[1 + \frac{l^2}{2k_{n+l}^2 R_0^2} \right] \right] \left[\frac{\alpha_+^2}{\omega \pm \Omega_2 - k_{n+l} v_{\parallel}} + \frac{\alpha_-^2}{\omega \mp \Omega_2 - k_{n+l} v_{\parallel}} \right], \quad (61)$$

where $\Phi \equiv 1 + \lambda_0^2 Q(\lambda_0)$. Observe that for all cases of practical interest $v_w \ll c$ and $|\bar{V}_{l,\pm 1, n \mp 1}| \ll |\bar{W}_{l,\pm 1, n \mp 1}|$. As a consequence, the terms in $\bar{V}_{l,\pm 1, n \mp 1}$ can be ignored. This is equivalent to the neglect of any direct coupling between the electromagnetic modes $\delta A_{l,\pm 1, n \mp 1}^{(\pm)}$. In addition, we shall neglect the coupling to the $\delta A_{l,\mp 1, n \pm 1}^{(\pm)}$ modes, so that

$$\epsilon_{l,\pm 1, n \mp 1}^{(\pm)} \simeq \frac{2J_{l,\pm 1}(\xi_{n \mp 1}) J'_{l,\pm 1}(\xi_{n \mp 1})}{J_l(\xi_{n \mp 1}) \Gamma_{l,\pm 1, n \mp 1}^{(l)}} + \frac{\pi}{2} R_0 \Delta R \bar{\Lambda}_{l,\pm 1, n \mp 1}^{(\pm)}. \quad (62)$$

Within the context of this approximation, the dispersion equation is of the form

$$\epsilon_{l,n} = \frac{\lambda_0^2}{1 + \lambda_0^2} \Phi \frac{\omega_b^2}{2\gamma_0 c^2} \left[\frac{\pi}{2} R_0 \Delta R \right]^2 \frac{\omega^2}{\gamma_0^2 (\omega - k_{n+l} v_{\parallel})^2} \bar{\chi}_{l,n} \left[\frac{1}{\epsilon_{l+1, n-1}^{(+)}} + \frac{1}{\epsilon_{l-1, n+1}^{(-)}} \right]. \quad (63)$$

Finally, if the solution is restricted to the first quadrant in (ω, k_n) space, then $|\epsilon_{l-1, n+1}^{(-)}| \gg |\epsilon_{l+1, n-1}^{(+)}|$ and (63) can be approximated by

$$\epsilon_{l,n} \epsilon_{l+1, n-1}^{(+)} \simeq \frac{\lambda_0^2}{1 + \lambda_0^2} \Phi \frac{\omega_b^2}{2\gamma_0 c^2} \left[\frac{\pi}{2} R_0 \Delta R \right]^2 \frac{\omega^2}{\gamma_0^2 (\omega - k_{n+l} v_{\parallel})^2} \bar{\chi}_{l,n}. \quad (64)$$

The complete dispersion equation (48) has been solved numerically for $\gamma = 3.5$, $\omega_b / \gamma^{1/2} c k_w = 0.1$, $\Omega_w / \gamma c k_w = 0.05$, $\Delta R / R_0 = 0.1$, $k_w R_g = 1.5$, and a wide range of axial guide fields for both the TE₁₁ and TM₁₁ waveguide modes. It should be remarked before we proceed further with a description of the numerical analysis that each of the off-diagonal elements of the dispersion tensor in Eq. (48) is directly proportional to Φ and, hence, the coupling coefficient also depends upon this function. The variation of Φ with the axial guide field, therefore, provides valuable insight into the effect of B_0 on the radiation growth rate. To this end, we plot Φ versus $\Omega_0 / \gamma c k_w$ in Fig. 3, in which the distinction between the value of the function for group I and group II orbits is clearly made. As discussed in Sec. II, Φ is characterized by singularities for both groups of orbits at the transitions to orbital instability (13), which occur at $\Omega_0 / \gamma c k_w \simeq 0.75$ (group I orbits) and $\Omega_0 / \gamma c k_w \simeq 0.62$ (group II orbits) for the parameters considered. While the growth rates at these points are also singular, it should be recognized that the linear theory itself breaks down in the vicinity of the singularities and a fully nonlinear treatment is required. The difference between Φ in the present three-dimensional theory and the one-dimensional analog²⁰ lies, principally, in the fact that no orbital instability (hence, no singulari-

ty) occurs for the group II orbits in one dimension. In addition, Φ vanishes at $\Omega_0 / \gamma c k_w \simeq 1.25$ (group II orbits) and the growth rate may be expected to vanish at this point as well.

The growth rate $\text{Im} k_n / k_w$ is plotted versus $\omega / c k_w$ in Fig. 4 for the TE₁₁ mode and $\Omega_0 / \gamma c k_w = 0.0$ and 0.5. The waveguide cutoff occurs at $\omega / c k_w \simeq 1.23$ and the two peaks shown for each value of the axial guide field correspond to the upper and lower intersections between the space-charge wave and the waveguide mode. This figure represents the cases corresponding to group I orbits, and we observe that the unstable spectrum is quite narrow but tends to broaden slightly with increasing B_0 corresponding to decreases in v_{\parallel} as the transition to orbital instability is approached. In addition, the resonant frequency decreases relatively fast with increasing B_0 for the upper intersection, but is not very sensitive to the value of the guide field for the lower intersection. Finally, we observe that the two peaks are well separated and that the growth rate corresponding to the upper intersection is the larger of the two. The peak growth rates and corresponding frequency at peak growth are plotted in Fig. 5 versus $\Omega_0 / \gamma c k_w$, in which the singularity at $\Omega_0 / \gamma c k_w \simeq 0.75$ is evident and that the growth rate for the upper intersection exceeds that of the lower intersection over the entire range

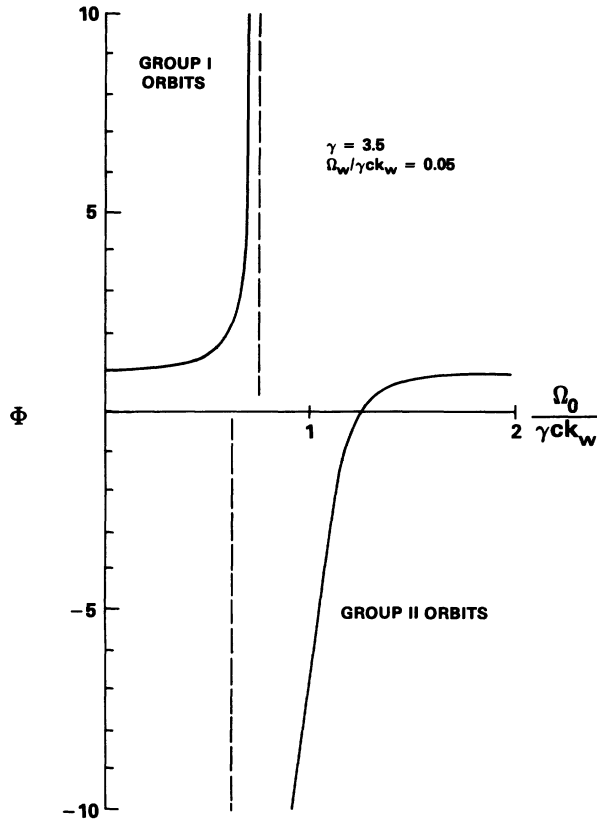


FIG. 3. Graph of $\Phi \equiv 1 + \lambda^2 Q(\lambda)$ vs the axial guide field for both group I and group II steady-state trajectories.

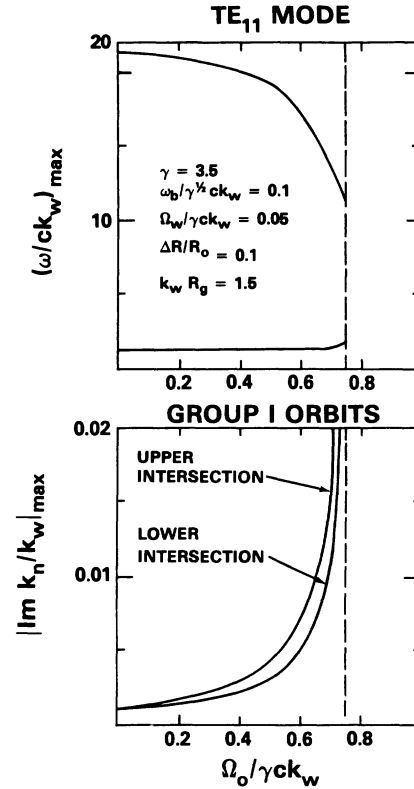


FIG. 5. Plots of the maximum growth rate and corresponding frequency for the TE₁₁ mode as a function of the guide field for group I orbits. Both the upper and lower intersections are shown.

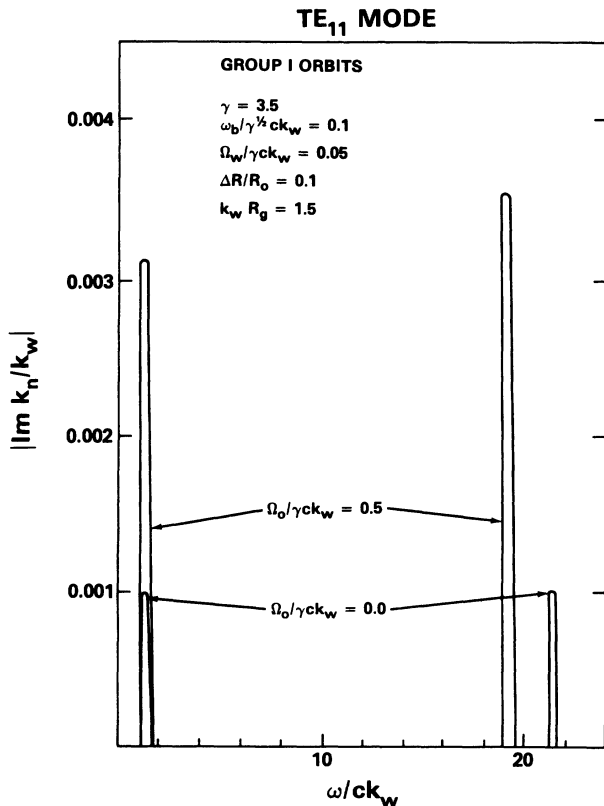


FIG. 4. Plot of the growth rate $\text{Im } k_n/k_w$ vs frequency for the TE₁₁ mode and group I orbits at $\Omega_0/\gamma ck_w = 0.0$ and 0.5.

of group I orbits. It is also clear that while the frequency at the upper intersection decreases with decreasing $v_{||}$, the frequency at the lower intersections increases. As a result, the interactions tend to coalesce with decreasing $v_{||}$; however, the cutoff of the TE₁₁ mode for the parameters considered is sufficiently low that coalescence does not occur for the group I orbits and the two lines remain well separated.

The growth rate for group II orbits is plotted versus frequency for $\Omega_0/\gamma ck_w = 1.0$ and 1.5 in Fig. 6 for the TE₁₁ mode. It is again clear that two peaks are found which correspond to the upper and lower intersections. However, in the case of $\Omega_0/\gamma ck_w = 1.0$ the axial velocity ($v_{||}/c \approx 0.87$) is sufficiently low that the two peaks are not well separated and overlap. This results in a substantially broadened spectrum of unstable waves. As the guide field is increased the axial velocity also increases and the separation between the peaks becomes more distinct. This is illustrated for $\Omega_0/\gamma ck_w = 1.5$ ($v_{||} \approx 0.95$) in which the two peaks are seen to be well separated. The peak growth rates and frequencies corresponding to the group II orbits are shown in Fig. 7 versus $\Omega_0/\gamma ck_w$. As in the case of group I orbits, the growth rates for the upper intersection everywhere exceed those of the lower intersection. In addition, it is clear that the growth rates vanish for $\Omega_0/\gamma ck_w \approx 1.25$ corresponding to the zero of Φ . Finally, it is seen that as $\Omega_0/\gamma ck_w$ decreases below unity the coalescence continues rapidly and the resonance is lost for

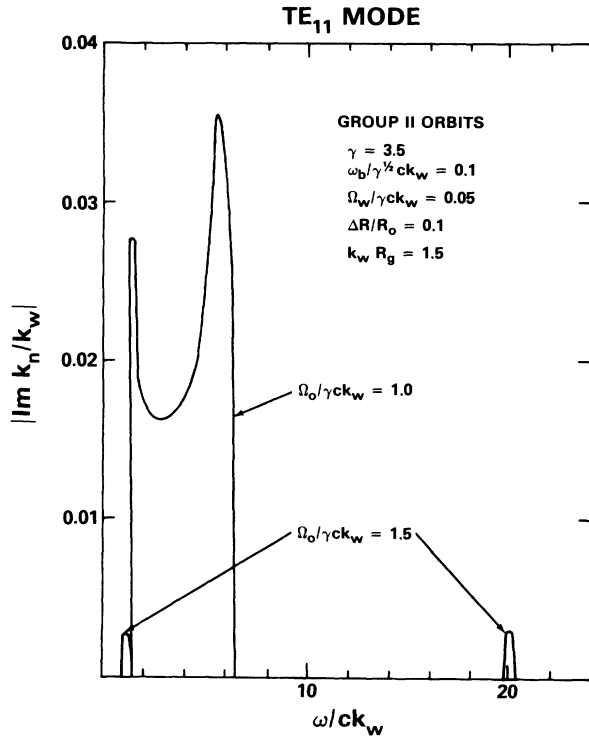


FIG. 6. Plot of the growth rate vs frequency for the TE₁₁ mode and group II orbits at $\Omega_0/\gamma ck_w = 1.0$ and 1.5 .

$\Omega_0/\gamma ck_w \leq 0.89$ by which point the double peak in the unstable spectrum has merged to form a single line. As a result, the interaction is lost at a value of the axial guide field greater than that corresponding to the singularity in Φ at $\Omega_0/\gamma ck_w \approx 0.62$ and no difficulties arising from the singularity occur.

One characteristic of the resonant nature of the interaction which must be emphasized is that the l th Doppler upshift describes interactions for all radial eigenmodes TE_{*lm*} and TM_{*lm*} ($m=1,2,3, \dots$). This constitutes a selection rule²⁴ which stems from the azimuthal variation of the steady-state orbits; specifically, that $\theta = k_w z$ and the phase of the waveguide modes varies as

$$\exp(ik_n z + il\theta - i\omega t) \sim \exp(ik_n z + ilk_w - \omega t).$$

The behavior of the growth spectrum for the TM₁₁ mode as a function of the axial guide field is qualitatively similar to that shown for the TE₁₁ mode. However, the TM₁₁ mode is characterized by a higher cutoff frequency (at $\omega/ck_w \approx 2.55$ for the parameters chosen); therefore, the upper (lower) intersection frequency is lower (higher) for the TM₁₁ mode than for the TE₁₁ at a given axial velocity. The maximum growth rate and corresponding frequency of the TM₁₁ modes are plotted versus $\Omega_0/\gamma ck_w$ in Figs. 8 and 9 for the group I and group II orbits, respectively. The growth rates are found to be comparable to those found for the TE₁₁ mode. It is evident, however, that the upper and lower intersections coalesce for the TM₁₁ before the singularity in Φ occurs on both the group I and group II orbits. Such coalescence was found only on the group

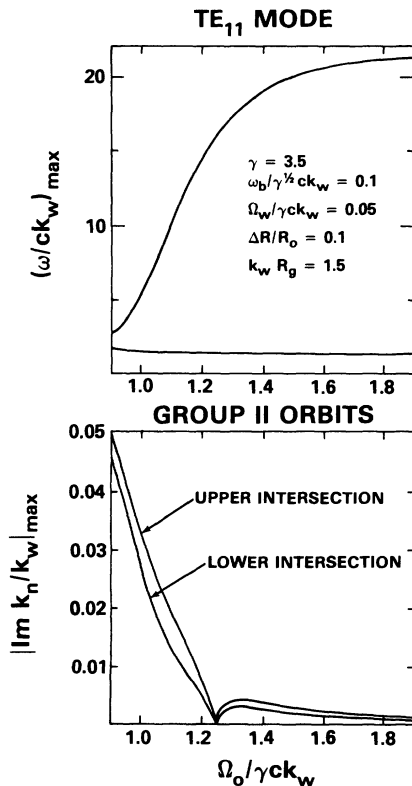


FIG. 7. Plots of the maximum growth rate and corresponding frequency for the TE₁₁ mode as a function of the guide field for group II orbits.

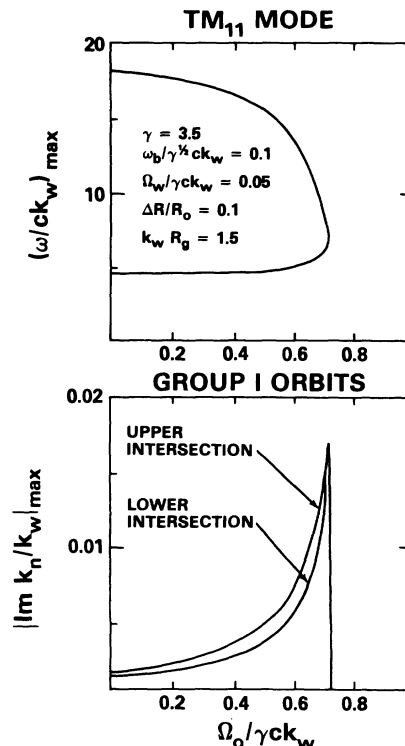


FIG. 8. Graph of the maximum growth rate and corresponding frequency for the TM₁₁ mode vs axial guide field for group I orbits.

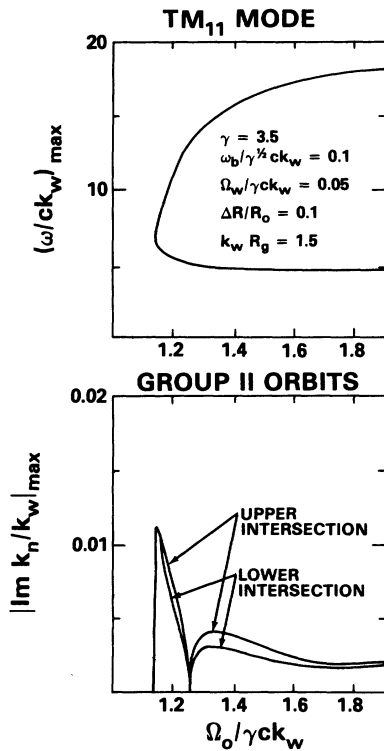


FIG. 9. Graph of the maximum growth rate and corresponding frequency for the TM_{11} mode vs axial guide field for group II orbits.

II orbits for the TE_{11} mode due to the lower value of the cutoff frequency.

VI. SUMMARY AND DISCUSSION

In this paper we have developed a collective theory of the free-electron laser which includes the effects of finite waveguide geometry and transverse gradients in the wiggler field. To this end, a Vlasov-Maxwell formulation has been employed which is equivalent to a perturbation expansion of the single-particle orbits to first order in the radiation and space-charge fields. The single-particle orbits are assumed to be helical, steady-state trajectories.^{24,27}

The principal difference between the orbits in the ideal (one-dimensional) and realizable (three-dimensional) wigglers is that in three dimensions unstable trajectories are found for both group I ($\Omega_0 < \gamma k_w v_{||}$) and group II ($\Omega_0 > \gamma k_w v_{||}$) orbits, while in one dimension only the group I trajectories can become unstable. Because of this feature, singularities are found in the linear growth rates for both types of trajectory in the realizable wiggler, which contrasts with the one-dimensional theory in which such a singularity occurs only for the group I class of orbit.

An additional feature of the three-dimensional theory arises from the fact that for given B_w , B_0 , λ_w , and γ at most one stable, steady-state orbit of each type exists. Thus for a specific guide and wiggler-field combination there is a unique mapping between γ and the orbit radius which implies that a nearly monoenergetic beam will be characterized by a small spread in the radii of the orbits described by the constituent electrons. As a result, we have solved the coupled Maxwell-Poisson equations in a "thin-beam" limit, and obtained the growth rates for the TE_{11} and TM_{11} modes. Wave amplification is found, in general, at both the upper and lower intersections of the waveguide and space-charge modes, although for sufficiently low axial velocities these two unstable regions of the spectrum are found to coalesce just prior to the point at which the intersections are lost.

It should also be reiterated that amplification of the TE_{lm} or TM_{lm} modes ($m=1,2,3,\dots$) occurs only for the resonance corresponding to the l th Doppler upshift. This constitutes a selection rule, and occurs because the azimuthal variation of the steady-state orbits varies as $\theta = k_w z$ and the phase of the waveguide modes vary as $\exp(ik_n z + il\theta - i\omega t)$. It is important to recognize, however, that not all beam electrons in an experimental device can be expected to execute the steady-state trajectories and, as a consequence, other waveguide modes (i.e., TM_{0m} or TE_{0m}) may be excited as well.

ACKNOWLEDGMENT

This work was supported in part by Naval Sea Systems Command and in part by Naval Electronic Systems Command.

*Permanent address: Science Applications, Inc., McLean, VA 22102.

¹L. R. Elias, W. M. Fairbank, J. M. J. Madey, H. A. Schwettman, and T. I. Smith, Phys. Rev. Lett. **36**, 717 (1976).

²D. A. G. Deacon, L. R. Elias, J. M. J. Madey, G. J. Ramian, H. A. Schwettman, and T. I. Smith, Phys. Rev. Lett. **38**, 892 (1977).

³V. L. Granatstein, S. P. Schlesinger, M. Herndon, R. K. Parker, and J. A. Pasour, Appl. Phys. Lett. **30**, 384 (1977).

⁴D. B. McDermott, T. C. Marshall, S. P. Schlesinger, R. K. Parker, and V. L. Granatstein, Phys. Rev. Lett. **41**, 1368 (1978).

⁵H. Boehmer, M. Z. Caponi, J. Edighoffer, S. Fornaca, J. Munch, G. R. Neil, B. Saur, and C. Shih, Phys. Rev. Lett. **48**, 141 (1982).

⁶J. M. Slater, IEEE J. Quant. Electron. **QE-17**, 1476 (1981).

⁷R. K. Parker, R. H. Jackson, S. H. Gold, H. P. Freund, V. L. Granatstein, P. C. Efthimion, M. Herndon, and A. K. Kinkead, Phys. Rev. Lett. **48**, 238 (1982).

⁸S. H. Gold, W. M. Black, H. P. Freund, V. L. Granatstein, R. H. Jackson, P. C. Efthimion, and A. K. Kinkead, Phys. Fluids **26**, 2683 (1983).

⁹P. Sprangle, V. L. Granatstein, and L. Baker, Phys. Rev. A **12**, 1697 (1975).

¹⁰P. Sprangle and V. L. Granatstein, Phys. Rev. A **17**, 1792 (1978).

¹¹T. Kwan and J. M. Dawson, Phys. Fluids **22**, 1089 (1979).

¹²I. B. Bernstein and J. L. Hirshfield, Phys. Rev. A **20**, 1661 (1979).

¹³P. Sprangle and R. A. Smith, Phys. Rev. A **21**, 293 (1980).

- ¹⁴R. C. Davidson and H. S. Uhm, *Phys. Fluids* 23, 2076 (1980).
- ¹⁵L. Friedland and J. L. Hirshfield, *Phys. Rev. Lett.* 44, 1456 (1980).
- ¹⁶H. P. Freund, P. Sprangle, D. Dillenburg, E. H. da Jornada, B. Liberman, and R. S. Schneider, *Phys. Rev. A* 24, 1965 (1981).
- ¹⁷I. B. Bernstein and L. Friedland, *Phys. Rev. A* 23, 816 (1981).
- ¹⁸H. S. Uhm and R. C. Davidson, *Phys. Fluids* 24, 1541 (1981).
- ¹⁹H. S. Uhm and R. C. Davidson, *Phys. Fluids* 24, 2348 (1981).
- ²⁰H. P. Freund, P. Sprangle, D. Dillenburg, E. H. da Jornada, R. S. Schneider, and B. Liberman, *Phys. Rev. A* 26, 2004 (1982).
- ²¹L. Friedland and A. Fruchtman, *Phys. Rev. A* 25, 2693 (1982).
- ²²W. A. McMullin and R. C. Davidson, *Phys. Rev. A* 25, 3130 (1982).
- ²³H. P. Freund, *Phys. Rev. A* 27, 1977 (1983).
- ²⁴H. P. Freund, S. Johnston, and P. Sprangle, *IEEE J. Quant. Electron.* QE-19, 322 (1983).
- ²⁵W. B. Colson and J. L. Richardson, *Phys. Rev. Lett.* 50, 1050 (1983).
- ²⁶L. Friedland, *Phys. Fluids* 23, 2376 (1980).
- ²⁷P. Diament, *Phys. Rev. A* 23, 2537 (1981).
- ²⁸H. P. Freund and A. T. Drobot, *Phys. Fluids* 25, 736 (1982).